LAWRENCE
LIVERMORE
NATIONAL
LABORATORY

UCRL-CONF-226068

Environmental and Geometrical Conditions to Sustain Crevice Corrosion in Alloy 22

R. M. Carranza, M. A. Rodríguez, R. B. Rebak

November 13, 2006

Corrosion/2007 Conference and Exposition
Nashville, TN, United States
March 11, 2007 through March 15, 2007

Paper 07581 prepared for presentation at the Corrosion/2007 Conference and Exposition, Nashville TN, 11-15 March 2007

ENVIRONMENTAL AND GEOMETRICAL CONDITIONS TO SUSTAIN CREVICE CORROSION IN ALLOY 22

Ricardo M. Carranza and Martín A. Rodríguez
Dep. Materiales, Comisión Nacional de Energía Atómica
Av. Gral. Paz 1499
B1650KNA San Martín, Buenos Aires, ARGENTINA

Raúl B. Rebak
Lawrence Livermore National Laboratory
7000 East Ave, L-631
Livermore, CA 94550, USA

ABSTRACT

Alloy 22 (N06022) is highly resistant to localized corrosion. Under aggressive environmental conditions Alloy 22 may be susceptible to crevice corrosion in hot chloride (Cl^-) solutions. The objective of the present work was to explore the environmental and geometrical conditions for crevice corrosion to occur. Electrochemical tests were performed using PCA and prismatic mill annealed Alloy 22 specimens in chloride solutions. Crevice corrosion current density was found to be a function of applied potential. i_{CREV} values ranged from 40 μA/cm^2 to 20 mA/cm^2. Such low values of current density explained the absence of pitting corrosion in Alloy 22 at any potential. Decreasing of the effective diffusion distance in a propagating crevice is thought to cause crevice corrosion stifling or repassivation after long anodic polarization. Crevice corrosion breakdown potential is expected to decrease with potential scan rate, approaching repassivation potential for low scan rates. The lowest corrosion potential of Alloy 22 in hydrochloric acid solutions at which active corrosion exists was proposed as the lowest possible repassivation potential for crevice corrosion.

Keywords: N06022, chloride, crevice corrosion, repassivation potential, geometry

INTRODUCTION

Alloy 22 (N06022) is a nickel (Ni) based alloy that contains nominally 22% Chromium (Cr), 13% Molybdenum (Mo) and 3% tungsten (W)[1]. Alloy 22 is one of the most versatile alloys of the Ni-Cr-Mo family and was designed to withstand the most aggressive industrial applications, including reducing acids such as hydrochloric and oxidizing acids such as nitric[2]. Nickel, the base element, is very resistant to hot alkalies, and the alloying elements chromium and molybdenum enhance its protection against oxidizing and reducing conditions respectively[2-4]. Alloy 22 has showed excellent resistance to pitting corrosion, crevice corrosion and environmentally assisted cracking in hot concentrated chloride solutions[2-4]. Applications of Alloy 22 include a variety of chemical processing, pickling and metal finishing, pollution control, nuclear waste treatment[3,4], pulp and paper industry and flue-gas desulfurization (FGD) plants[5]. Due to its excellent corrosion resistance in a wide variety of environments Alloy 22 has been selected for the fabrication of the corrosion-resistant outer shell of the high-level nuclear waste container for the proposed Yucca Mountain repository[6-8].

Alloy 22 can be considered not susceptible to pitting corrosion in most of practical applications in chloride containing environments[9]. However, Alloy 22 might suffer crevice corrosion under certain aggressive conditions[6-9]. The factors influencing crevice corrosion susceptibility of Alloy 22 has been discussed by Rebak[9] and can be classified into environmental (external) and metallurgical (internal)[6,9]. External factors include[9] chloride concentration, temperature, applied potential, presence of inhibitors or deleterious species, pH, microbial activity, volume of electrolyte, crevice former geometry, crevicing material, etc. Internal factors include[9] the metallurgical condition of the alloy (microstructure), presence of a weld seam, type of annealing, oxide film formed, surface finishing, etc. Many of the factors listed above such as chloride concentration, temperature, presence of some inhibitors, metallurgical condition of the alloy and presence of a weld seam have been studied in some detail[10-24]. The influences of other factors such as crevice former geometry and crevicing material still need to be investigated[9].

Figure 1 shows a schematic representation of a crevice showing the two characteristic dimensions, the crevice depth (x) and the crevice gap (g). Parameters commonly used as scaling factors for correlations in the study of geometrical aspects of crevice corrosion are the ratios x^2/g and x/g[25-29]. Vankeerberghen[28] studied the effect of crevice geometry on crevice corrosion of mild steel in sodium acetate-acetic acid buffer and aluminum in sodium chloride. Different macroscopic crevicing mechanisms were used. It was determined that there is a critical characteristic dimension, $x^2/g > (x^2/g)_{CRIT}$, that marks the limit between crevices that show or do not show crevice corrosion. Lee *et al.*[27] studied crevice corrosion scaling factors on Ni200 in 0.5M H_2SO_4. Microfabrication methods were used to construct crevice formers of rigorously controlled gap and depth. Crevice formers with gaps as low as 7 μm were fabricated using this technique. They found that x^2/g is the fundamental controlling scaling factor and capillary forces became important for small gap crevices. However, some of these metal-environment systems studied[27,28] (such as mild steel in sodium acetate-acetic acid buffer and Ni200 in 0.5M H_2SO_4) do not show pitting corrosion and are characterized by the presence of an active to passive transition peak in their corresponding anodic polarization curve[29]. Crevice corrosion can be rationalized as a result of an ohmic drop (IR drop) which leads potential inside the crevice in the active zone for deep enough crevices[26,29]. Other metal-environment systems such as stainless steel and nickel-chromium alloys in near neutral chloride solutions do not show an active to passive transition. A simple ohmic drop without a significant chemistry change in the local environment cannot cause crevice corrosion in these systems[29]. Be-

sides, the relationship between pitting and crevice corrosion for stainless steel and nickel-chromium in chloride solutions alloys has been recognized by many authors[29]. Effects of geometrical scaling factor on crevice corrosion of systems where ohmic drop is not necessarily the controlling mechanism still need to be investigated.

Most of the crevice corrosion studies for Alloy 22 involved the used of artificially creviced specimens. The crevicing mechanism commonly used is based on ASTM G 48[1] which contained 24 artificially creviced spots formed by PTFE (polytetrafluoroethylene) washers or PTFE-wrapped ceramic washers. These specimens include multiple crevice assemblies (MCA) [10,11,15-19] and prism crevice assemblies (PCA)[20,21,23,24]. Different amounts of torque were applied to the washers to obtain a tight crevice[10,11,15-24]. However, the depth and the gap of the obtained crevice have never been quantified[9]. It has been recently argued that PTFE-wrapped ceramic washers are more demanding that PTFE washers[9,20,24]. Pressure applied to the latter can relax in time as PTFE is a polymeric material[24]. Another type of specimens which contains an artificial crevice formed by a PTFE compression gasket is a variation of the ASTM G 5[1] specimen usually referred to as prismatic[12,14,22,30]. This type of PTFE compression gasket is not considered demanding enough to study crevice corrosion of Alloy 22.[30]

The corrosion degradation model for the Yucca Mountain nuclear waste container assumes that localized corrosion will only occur when the corrosion potential E_{CORR} is equal or greater than a critical potential (E_{CRIT})[6,13]. That is, if $E_{CORR} < E_{CRIT}$, general or passive corrosion will occur and localized corrosion is not expected[6]. In environments that promote localized corrosion, E_{CRIT} is the lowest potential that would initiate crevice corrosion[6]. The use of critical potentials to establish a lower bound parameter below which localized corrosion does not occur has been discussed by Sridhar and Cragnolino[31]. They established that pitting repassivation potential (E_{RP}) is independent of previous pit growth if the circulated anodic charge density is higher than a certain threshold value for Alloy 825 and 316L stainless steel[31]. If relatively deep pits are considered E_{RP} is independent of prior pit growth. The authors pointed out that deep pits are similar to crevices and so repassivation potential for crevice corrosion is independent of previous crevice growth[31]. Repassivation potential for crevice corrosion of Alloy 22 has been determined in different experimental conditions in a wide variety of works[6,9,10-13,15-20,22-24]. This parameter is usually extracted from cyclic potentiodynamic polarization curves (CPP) using artificially creviced specimens[6,9]. This technique was first introduced by Wilde and Williams[32] and was standardized by ASTM[1]. Alternative techniques are also used as Tsujikawa-Hisamatsu electrochemical method (THE)[16,20] and potential step methods[16,18,19]. Repassivation potentials for Alloy 22 in near neutral hot chloride solutions have been determined in different laboratories[9,11,19,23,24]. This parameter decreased with increasing chloride concentration and temperature[9]. Repassivation potentials determined in different laboratories are in agreement when the same crevicing mechanism is used[24]. Values obtained using PTFE-wrapped ceramic washers are lower than those obtained with PTFE washers at the same applied torque[24]. There was a very good agreement between repassivation potential determined by CPP and THE[20].

Localized acidification model developed by Galvele[33-35] establish that the pitting potential (E_P) of a metal or alloy in a near neutral solution can be evaluated from the anodic behavior of the same metal in a low pH solution. According to this model the pitting potential is given by[33]

$$E_P = E_C^* + \eta + \Phi \qquad (1)$$

where E_C^* is the corrosion potential in the acidified solution, η is the polarization necessary to obtain a current density high enough to maintain acidity inside the pit and Φ is the potential drop inside the pit. The value of η depends on $x.i$, where x and i are the diffusion distance and the current density into the pit, respectively. The same equation can be used to evaluate the repassivation potential for pitting or crevice corrosion[31]. Localized acidification model has successfully explained several experimental observations on pitting and crevice corrosion of pure metals and alloys[33-39]. Results of the present work are discussed in terms of this model.

The aim of the present work was to explore the environmental and geometrical conditions for crevice corrosion to occur on Alloy 22 in hot chloride solutions at 90°C.

EXPERIMENTAL PROCEDURE

Alloy 22 (N06022) specimens were prepared from wrought mill annealed plate stock. The chemical composition of the alloy in weight percent was 59.56% Ni, 20.38% Cr, 13.82% Mo, 2.64% W, 2.85% Fe, 0.17% V and 0.16% Mn, 0.008% P, 0.0002% S, 0.05% Si, and 0.005% C (Heat 059902LL1). All the tested material was wrought Mill Annealed (MA). Two different types of specimens were used: (a) prismatic specimens: a variation of the ASTM G 5[1] specimen, which contained an artificial crevice formed by a PTFE compression gasket; and (b) prism crevice assemblies (PCA), fabricated based on ASTM G 48[1] which contained 24 artificially creviced spots formed by a ceramic washer (crevice former) wrapped with a PTFE tape. The applied torque was 7.92 N-m (70 in-lb). The PCA specimen has been described before[20,21,23,24]. The tested surface areas were approximately 10 cm^2 for prismatic specimens and 14 cm^2 for PCA specimens. The specimens had a finished grinding of abrasive paper number 600 and were degreased in acetone and washed in distilled water 1 hour prior to testing. Nitrogen (N_2) was purged through the solution 1 hour prior to testing and was continued throughout the entire test, for tests performed in deaerated conditions. Natural aeration was allowed throughout the entire test for tests performed in aerated solutions.

Electrochemical tests were carried out using PCA specimens in deaerated pH 2, 1M NaCl at 90ºC. These tests consisted in:

1) Corrosion potential monitoring during 15 minutes of immersion.

2) Potentiostatic hold at a fixed applied anodic potential between -200 mV_{SCE} to 700 mV_{SCE} for a period of time enough to produce propagation of crevice corrosion.

3) Electrochemical impedance spectroscopy (EIS) measurement at the corresponding applied potential.

4) Potentiostatic hold at the corresponding applied potential.

5) Potentiodynamic polarization scan at 0.167 mV/s in the cathodic direction until repassivation is reached (that is, until cathodic current higher than 1 $\mu A/cm^2$ is measured).

Potentiodynamic polarization tests were performed using prismatic specimens in 5M HCl, 3M HCl, 1M HCl and 0.1M HCl + 0.9M NaCl deaerated solutions at 90ºC. The potential scan was started 5 mV below the corrosion potential (E_{CORR}) in the anodic direction at a

scan rate of 0.167 mV/s. A potentiostatic hold was performed for 5 minutes at the onset potential (5 mV below E_{CORR}) before starting the scan. The test was finished when the current density reached a value of 1 to 50 mA/cm^2 depending on HCl concentration.

Monitoring of corrosion potential (E_{CORR}) and electrochemical impedance spectroscopy (EIS) measurements for different immersion times were carried out using prismatic specimens in low pH chloride aerated and deaerated solutions at 90ºC. These solutions include different mixtures xM NaCl + yM HCl with pH values ranging from 0.1 to 2 (with x + y = 1M) and also hydrochloric acid solutions with concentrations ranging from 1M to 5M.

For the electrochemical impedance spectroscopy (EIS) measurements a 10 mV amplitude sinusoidal potential signal was superimposed to the corrosion or applied potential. The frequency scan was started at 10 kHz and ended at 1 mHz. In the case of measurements at E_{CORR}, the parameters of simple equivalent circuit mathematical models were fitted to these data in order to obtain polarization resistances (R_P) which led to instantaneous uniform corrosion rates. The Tafel constants, β_A and β_C, were assumed to be ± 0.12 V/decade for the calculation of the corrosion currents from R_P values. These values do not imply the assumption of any corrosion mechanism, they are just the most common values used in literature.

Corrosion rates were calculated using Equation (2)

$$CR(mm/yr) = \frac{K\, i_{CORR}\, EW}{\rho} \qquad (2)$$

where i_{CORR} is the passive corrosion current density in A/cm^2, EW is the equivalent weight, K is the faradaic conversion factor (3,270 mm g A^{-1} cm^{-1} yr^{-1}) and ρ is the density (8.69 g/cm^3 for Alloy 22). Assuming congruent dissolution of the major alloying elements as Ni^{2+}, Cr^{3+}, Mo^{6+}, Fe^{3+}, and W^{6+} the EW for Alloy 22 is 23.28[1].

All the electrochemical tests were conducted in a one-liter, three-electrode vessel (ASTM G 5)[1] A water-cooled condenser combined with a water trap was used to avoid evaporation of the solution and to prevent the ingress of air (oxygen). The temperature of the solution was controlled by immersing the cell in a thermostatized bath, which was kept at a constant temperature of 90ºC. All the tests were performed at ambient pressure. The reference electrode was a saturated calomel electrode (SCE), which has a potential of 0.242 V more positive than the standard hydrogen electrode (SHE). The reference electrode was connected to the solution through a water-cooled Luggin probe. The counter electrode consisted in two connected flags of platinum foil (total area 100 cm^2) spot-welded to a platinum wire. All the potentials in this paper are reported in the SCE scale.

After the electrochemical tests, all the specimens were examined in an optical microscope (OM) to establish the mode, location and depth of the attack, in those cases that localized attack was produced. Some of the specimens were observed in the scanning electron microscope (SEM).

RESULTS

Tests on prism crevice assemblies (PCA) specimens

Figure 2 shows potentiostatic polarization curves for Alloy 22 PCA specimens in pH 2, 1M NaCl solutions at 90ºC and at different anodic applied potentials. Two different regions can be distinguished at each applied potential. The first region is characterized by a linear decrease of log (i) with log (t). This is related with formation of a passive film (*i.e.* passivation)[21]. The second region is characterized by an increase of current in time, and this is the onset of crevice corrosion[21]. Time required for crevice corrosion onset decreased for increasing anodic applied potentials. In general, the current density value reached at the end of the polarization increased with an increase of anodic applied potential.

Figure 3 shows linear fittings of log (i) with log (t) curve in Region 1 and part of Region 2 for the Alloy 22 PCA specimen polarized at -100 mV_{SCE}. The time corresponding to the intersection of the two fitted lines for regions 1 and 2 was defined as the incubation time (t_{INC}) for the onset of crevice corrosion. Figure 4 shows incubation time as a function of the applied potential. A linear decrease of log(t_{INC}) with potential was observed from -170 mV_{SCE} to 200 mV_{SCE}. For higher potentials, the onset of crevice corrosion occurred immediately, and the observed t_{INC} was about a minute. For potentials lower than -170 mV_{SCE} (*i.e.* -180 mV_{SCE} and -200 mV_{SCE}) no crevice corrosion was detected in spite of the longer polarization times.

Figure 5 shows complex plane impedance plots for EIS measurements at different applied potentials and polarization times. These curves show a depressed semi-circle aspect for all the potentials, which is a typical behavior of charge transfer controlled processes. The size of the depressed semi-circles decreased as applied potential increased indicating an increasing rate of the charge transfer process. No indication of a diffusion controlled process can be detected from these impedance diagrams. However, a non-steady state of crevice corrosion propagation could have masked a diffusion controlled process in the low frequency part of the diagram.

Figure 6 shows the repassivation curves for all the initial applied potentials. These curves are cathodic potentiodynamic polarization curves started after potentiostatic holding at different anodic potentials (step 5 in experimental procedures). The shape of these curves was the same for all tested potentials and it did not depend on initial applied potential. A new corrosion potential (zero current) was built up at the end of these scans. This corrosion potential was generally higher for the higher applied potentials. A repassivation potential criterion usually taken in cyclic potentiodynamic polarization curves is E_{R1}[9,23]. This is the potential at which the current density reaches 1 $\mu A/cm^2$ in the reverse scan. Figures 7 and 8 show E_{R1} as a function of the applied potential and the total circulated anodic charge (potentiostatic hold plus potentiodynamic scan) respectively. E_{R1} shows a scatter of approximately 40 mV. The highest E_{R1} corresponded both to the higher applied potentials and circulated charges.

Figures 9 and 10 show photographs of PCA specimens after testing along with the corresponding contours of the creviced corroded areas. Specimen surfaces that suffered crevice corrosion are shown for specimens tested at 100 mV_{SCE} and 500 mV_{SCE}. Contours of creviced corroded areas where obtained by using an image processing software[(1)]. Localized corroded areas were calculated with these contours and they are listed in Table 1 for each applied po-

[(1)] ImageJ® 1.32j - Wayne Rasband National Institute of Health, USA. This software is in the public domain.

tential. Crevice corrosion appeared as a localized attack under the ceramics crevice formers (Figures 9 and 10). For applied potentials higher than 300 mV_{SCE}, crevice corrosion was also found under the top PTFE compression gasket. Microscopic observations (Figures 11-14) indicated that grains of the alloy were discernible as well as crystal planes. The morphology of attack was described as crystalline[9]. This attack seems to follow the higher energy planes in the crystal structure of the grains, and therefore the low energy planes are left visible on the corroded surface.[9]. Maximum depths of attack detected by optical microscopic observation for each test and other relevant information are listed in Table 1. Depth of attack can be roughly correlated with circulated charge and applied potential (Table 1). Higher depths of attack were found for higher circulated charges and applied potentials. Pitting corrosion was not observed in any case. A dark precipitate was found around the localized attacked areas (Figures 9-14) and sometimes also covering them. Energy Dispersive x-ray (EDX) analyses were performed in the scanning electron microscope (SEM) in order to detect the elements present in these precipitates. Results are listed in Table 2. Besides the constituents of Alloy 22 (Ni, Cr, Mo, W, Fe and Mn) chlorine (Cl) and silicon (Si) were detected. Chlorine was present in the solution (as chloride) and silicon could have proceeded from the glass cell. Table 3 shows the ratio of atomic percent of the element present in the precipitate and atomic percent of the element nominally present in Alloy 22. The elements W and Mo are highly enriched in the precipitate, Fe is present in the same amount as in the alloy, Cr is slightly depleted and Ni is highly depleted in the precipitate. As the solutions used in these work were not buffered, some changes in the pH value were detected at the end of each CPP. Final pH value ranged from 1.8 to 2.1.

Figure 15 shows the estimated current density on the crevice corroded area (i_{CREV}) as a function of anodic applied potential. This current density (i_{CREV}) was calculated as the ratio of the total current at the end of the potentiostatic hold and the creviced corroded area (Table 1) for each potential. Further details and discussion about this calculation are given in the following section. i_{CREV} showed a Tafel-like dependence with potential between -170 mV_{SCE} and 300 mV_{SCE} and its value became independent of applied potential (about 20 mA/cm^2) for higher potential values. i_{CREV} showed a small drop for the highest applied potential (700 mV_{SCE}).

Tests on prismatic specimens

Figure 16 shows corrosion potential values (E_{CORR}) of prismatic Alloy 22 specimens tested in aerated and deaerated chloride solutions as a function of pH or proton activity (a_{H^+}). E_{CORR} increased with time for aerated solutions of pH higher than approximately 0.3 (not shown) so the maximum reached E_{CORR} is plotted (usually the value reached at the end of the test) in Figure 16. On the other hand, E_{CORR} remained constant in time for deaerated solutions of pH lower than 1.7 (not shown) so the average E_{CORR} is plotted in Figure 16. E_{CORR} remained constant in time for aerated and deaerated solutions of pH lower than 0.3 (not shown). These solutions include hydrochloric acid of concentrations ranging from 1M to 5M. pH values for these solutions were corrected on account of chloride effect on proton activity.[40] E_{CORR} drop as pH decreased in aerated solutions (Figure 16) indicates a transition from passive to active state. A depassivation pH (pH_D) can be defined as the pH value at which this potential drop takes place. In this case pH_D is about 0.3 (Figure 16). In deaerated solutions such a transition is not evident from this plot (Figure 16). E_{CORR} in concentrated hydrochloric acid solutions seemed to be set by the hydrogen cathodic reaction as it showed a pH dependence similar to the thermodynamically predicted dependence for this reaction[41] (Figure 16).

Figure 17 shows corrosion current density (i_{CORR}) and corrosion rate (CR) of prismatic Alloy 22 specimens determined from EIS measurements in low pH chloride solutions as a function of hydrochloric acid concentration or pH. In this case pH values were not corrected for hydrochloric acid concentration higher than 1M. Total chloride concentration for solutions of pH > 0 ([HCl] < 1M) was always made equal to 1M by NaCl additions. Results obtained by Rebak and Crook[42] in similar conditions (boiling HCl solutions) are also plotted for comparison in Figure 17. CR in concentrated hydrochloric acid solutions ranged from 1 to 20 mm/year. There were no significant differences between aerated and deaerated conditions for these solutions. CR in aerated conditions showed a sudden decrease from 0.6M HCl + 0.4M NaCl (pH 0.22) to 0.5M HCl + 0.5M NaCl (pH 0.3). This decrease in CR can be correlated with the E_{CORR} drop in aerated solutions (Figure 16) at pH_D, *i.e.* it is related with active to passive transition. CR in deaerated conditions showed a gradual decrease as [HCl] decreases in a wide range of hydrochloric acid concentration followed by a drop from 0.02M HCl + 0.98M NaCl (pH 1.7) to 0.01M HCl + 0.99M NaCl (pH 2) (Figure 17). Similar CR values were found in aerated and deaerated pH 2 chloride solutions. These results indicates that Alloy 22 is in active state at pH > pH_D in deaerated solutions. The active to passive transition in deaerated solutions occurs at a pH of about 1.7 (Figure 17). Active state is never expected to exist in solutions of pH > 1.7 both in aerated and deaerated conditions.

Figure 18 shows potentiodynamic polarization curves of Alloy 22 prismatic specimens in hydrochloric acid solutions of different concentrations. These curves were corrected for ohmic drop. E_{CORR} obtained from polarization curves increased with increased HCl concentration in coincidence with open circuit tests (Figure 16). An active anodic peak followed by a wide passivity or pseudo-passivity range and a further current increase was found in the polarization curves in 3M HCl, 1M HCl and 0.1M HCl + 0.9M NaCl. A continuous current increase was found in 5M HCl (no passivation). A Small shallow peak was detected in the passivity or pseudo-passivity range of polarization curves in 3M HCl and 1M HCl solutions. Crevice corrosion attack was found under the PTFE compression gasket in these specimens. The specimens tested in 3M HCl and 0.1M HCl + 0.9M NaCl did not suffer any localized attack. A thin non-adherent dark oxide was found on the surface of all the specimens after testing.

DISCUSSION

The average values for critical potentials, namely breakdown (E_{20})[12,23] and repassivation (E_{R1}) potentials extracted from CPP for Alloy 22 in deaerated pH 6, 1M NaCl at 90ºC are reported to be E_{20} = 0.216 V_{SCE} and E_{R1} = –0.139 V_{SCE}[23]. Their corresponding standard deviations were 0.100 V (E_{20}) and 0.008 V (E_{R1}) [23]. Experimental conditions of the present work can be considered the same as those previously reported[23] as E_{R1} was found to be independent of pH in a wide range of values from pH 1 to pH 12.[43] Kehler *et al.* found that critical potentials are independent of pH value in the range from pH 2.75 to pH 7.75 for alloys 625 and 22 at in slightly different conditions[11]. Constant potential tests from the present work indicated that the lowest potential value for crevice corrosion to occur was –0.170 V_{SCE} (Table 1). Repassivation potentials (E_{R1}) determined after significant crevice growth was in the range of –0.200 V_{SCE} to –0.140 V_{SCE} (Figures 7 and 8). These E_{R1} are slightly lower but consistent with reported values[20,23]. E_{R1} seemed to increase for increasing circulated charge densities (CD) (Figures 8). Contrarily to this observation, E_{R1} has been reported to decrease when higher current densities are reached in the forward scan of CPP.[32] Kehler *et al.* reported that repassivation potentials are independent of CD associated with crevice attack in the entire studied range (10^{-1}–10^{3} C/cm^2 for Alloy 625 and 10^{-2}–10^{2} for Alloy 22)[11]. Sridhar and Cragnolino[31] found that pitting

repassivation potential for Alloy 825 and 316L stainless steel decreases for increasing circulated CD and remains constant for circulated CD higher than a threshold value. These observations has been explained by Galvele's localized acidification model[31,33]. As pit depth increases, the diffusion distance into the pit (x) also increases and less current density (i) is required to maintain the critical conditions for the localized corrosion to occur ($x.i > (x.i)_{CRIT}$)[33]. As current density in the pit-like solution is a function of applied potential (usually a Tafel relationship) the required potential to sustain localized acidification also decreases.[33] Sridhar and Cragnolino[31] explained the existence of a minimum repassivation potential for pitting corrosion after a threshold CD by considering negligible the polarization term (η) in Equation 1 for deep enough pits and also by considering the potential drop (Φ)constant and equal to the ohmic drop in a precipitated salt film inside the pit. In these conditions Equation 1 becomes Equation 3.

$$E_{RP} = E_C^* + \Phi \qquad (3)$$

Let us suppose x^2/g is the controlling scaling factor for this metal-environment system, although the following analysis is valid if x/g is the controlling scaling factor. As Galvele's model is unidimensional[33], the diffusion distance (x) should be replaced by an effective diffusion distance (x^2/g) which takes into account the effect of crevice gap. Then the critical condition for the localized corrosion to occur can be re-written as ($x^2 i/g > (x^2 i/g)_{CRIT}$). Geometrical conditions in a propagating crevice may be different from a developing pit. Figure 19 depicts a two-stage localized corrosion process in a deep pit and in a crevice. In the first case effective diffusion distance (x^2/g) into the pit is increased by corrosion while in the latter, x^2/g into the crevice is decreased by corrosion. Diffusion path in a crevice is created by the surface placed on the metal (*i.e.* crevice former or compression gasket) and it is not increased by further crevice corrosion. Crevice corrosion stifling or repassivation observed by Yilmaz *et al.*[21] after long polarization of artificially creviced Alloy 22 PCA specimens can be attributed to progressive increasing of the crevice gap (g) that causes a decrease in x^2/g, x remaining approximately the same during the entire test.

Development of crevice corrosion not only results in a decrease of the effective diffusion distance (x^2/g) but also results in the production of an increasing amount of protons (H^+) in the occluded solution. These protons will be reduced to hydrogen when the scan is reversed to the cathodic direction, producing a cathodic current superimposed to the crevice corrosion current. The total current (I) measured during repassivation (*i.e.* reverse scan of CPP) can be expressed as follows (Equation 4).

$$I = i_{PASS} \cdot A + i_{CREV} \cdot A_{CREV} - i_{H^+/H_2} \cdot A_{CREV} \qquad (4)$$

Where i_{PASS} is the passive current density, A is the specimen total area, i_{CREV} is the anodic current density in the crevice, A_{CREV} is the area which suffers crevice corrosion and i_{H^+/H_2} is the hydrogen reduction current density within the crevice. The condition for repassivation to be reached is $I = i_{PASS} \cdot A$, which can be fulfilled if the second and third terms of Equation 4 cancel each other. Significant hydrogen evolution in the occluded cell results in an early determination of repassivation at potentials where i_{CREV} is not null.

A higher repassivation potential for higher applied potentials and higher circulated charges (Figures 6, 7 and 8) can be a result of these two factors: increasing of effective diffusion distance (x^2/g) and significant hydrogen evolution within the crevice.

Differences between breakdown and repassivation potentials of crevice corrosion can be attributed to the potentiodynamic nature of the scan in CPP, taking into account the effect of potential in incubation time (Figure 4). Breakdown potential is expected to decrease, and therefore to approach the repassivation potential, for low scan rates.

Total current (I) measured at different polarization times (t) in the constant potential tests (Figure 2) can be expressed as follows (Equation 5), neglecting cathodic reactions within the crevice.

$$I(t) = i_{PASS}(t) \cdot A + i_{CREV} \cdot A_{CREV}(t) \quad (5)$$

Current density in the crevice (i_{CREV}) can be considered only a function of potential. Galvele *et al.*[36] studied pitting of 18%Cr-x%Mo ferritic stainless steels in chloride solutions. They calculated pitting current densities as a function of potential in 1M HCl by measuring the depth and the diameter of the pits under a microscope at 100 times. Under this consideration i_{CREV} can be expressed as follows (Equation 6).

$$i_{CREV} = \frac{I(t) - i_{PASS}(t).A}{A_{CREV}(t)} \quad (6)$$

Three characteristic domains are found in these tests[21]: (Region 1) passivation, (Region 2) crevice corrosion nucleation and growth, and (Region 3) crevice corrosion stifling or repassivation. The objective of the present work was to determine i_{CREV} as a function of potential. In this work, the applied potential was maintained until reaching Region 2 in potentiostatic tests. An increase of I in Region 2 was considered to be a result of an increase of A_{CREV}, being i_{CREV} approximately constant in time. The term $i_{PASS}(t) \cdot A$ becomes negligible for large polarization times in Region 2, so Equation 6 becomes Equation 7,

$$i_{CREV} = \frac{I}{A_{CREV}} \quad (7)$$

where I was obtained from the final value of the current in the constant potential tests (Figure 2) and A_{CREV} was calculated from contours of creviced areas obtained with an image processing software (Figures 9 and 10). Increasing of crevice corroded area during potentiodynamic cathodic scan was neglected. Obtained corroded areas ranged from 0.30 to 0.75 cm^2 (Table 1) with an estimated error of 0.02 cm^2. Calculated i_{CREV} values have an error of the same order of magnitude than corresponding corrosion rate measured by electrochemical methods.

Figure 20 shows i_{CREV} as a function of potential along with the active range in polarization curves of Alloy 22 in different HCl solutions. Since the corrosion behavior of a metal in an active crevice is known to be correlated to its anodic behavior in the active condition in a low pH solution[33] this comparison may be useful. Low pH solution in the crevice results from metal cation hydrolysis.[25,31,33] Precipitation of salts is expected because of the high concentrations of

metallic cations and chlorides.[25,31,33] Solution chemistry inside the crevice is more complex than the pure hydrochloric acid solutions used for comparison. Nevertheless, pure hydrochloric acid solutions have been used to simulate the conditions in active pits, specially in order to obtain E_C^* for the localized acidification model[36-39]. Galvele *et al.*[36] considered 1M HCl was representative of the pit-like solution of 18%Cr-x%Mo ferritic stainless steels in 1M NaCl. Newman[38] studied the anodic behavior of Fe-Cr-Ni alloys in 1M and 4M HCl solutions using the scratching technique to establish the effect of molybdenum in pitting of stainless alloys. If anodic behavior of Alloy 22 in pure hydrochloric acid solutions is considered to be representative of the anodic response in the crevice solution, the curve i_{CREV} vs. E can be interpreted as a polarization curve in HCl (Figure 20) distorted by significant potential drop inside the crevice. A large potential drop is expected because of the presence of a salt film layer precipitated on the metal in the crevice corroded area[31] as it was shown in the present work (Figures 9-14).

Corrosion kinetics in the crevice solution can involve very complex processes. Only charge transfer processes were detected by EIS (Figure 5) and it is reasonably to consider that charge transfer is the rate controlling step of the corrosion process for low polarizations (Figure 15) where a Tafel-like dependence was found. For higher polarizations diffusion processes may become the rate controlling step (Figure 15), but no evidence was found (Figure 5). Ohmic control may also become the rate controlling step for higher polarizations, as the potential drop in the salt layer deposited on the crevice is thought to be large.[31]

The maximum current density measured inside an active crevice was about 20 mA/cm^2 (Figure 20). Current densities for active pits in other metal-environment systems are reported to be higher[33]. Galvele[33] reviewed current densities inside pits of pure metals and alloys. They range from 0.1 to 70 A/cm^2, most of them at room temperature. Current densities higher than 1 A/cm^2 were found for ferritic stainless steels in 1M HCl[36]. They seem to increase monotonically with potential. Compared with data for stainless steels[36], current densities for crevice corrosion of Alloy 22 in NaCl solution at 90ºC can be considered very low. Since the maximum i_{CREV} did not exceed 20 mA/cm^2 at any applied potential, this could explain the fact that no pitting corrosion has been detected in these conditions[9,23]. A critical x.i value must be reached for the pitting corrosion to take place[33]. Since i_{CREV} (in this case i_{PIT}) cannot be higher than 20 mA/cm^2 and diffusion distance (x) provided by passive film rupture is limited by surface roughness, it is possible that the above critical conditions cannot be reached at any applied potential.

It is interesting to analyze the existence of a minimum limiting repassivation potential value for crevices with $x^2/g \to \infty$, *i.e.* independent of crevice geometry. Equation 3, obtained by Sridhar and Cragnolino[31] by neglecting the polarization term of Galvele's equation[33], can be further reduced to Equation 8 by considering the potential drop term also negligible. This assumption is reasonable for Alloy 22 at low polarization potentials in concentrated chloride solutions, taking into account the low i_{CREV} (about 40 μA/cm^2) reached at –0.170 V_{SCE} (Figure 15).

$$E_{RP} = E_C^* \qquad (8)$$

Equation 8 shows that this limiting crevice corrosion repassivation potential is equal to the corrosion potential in the crevice solution. Let us consider the reverse scan in a CPP performed in an artificially creviced Alloy 22 specimen tested in a near neutral chloride concentrated solution after crevice corrosion was allowed to propagate for certain time. Let us as-

sume the geometrical conditions in the crevice are such that $x^2/g \to \infty$. When the current density in the crevice solution is low enough for Equation 8 to be valid, the applied potential should be about –0.170 V_{SCE} (low current density and therefore no significant ohmic drop). This potential value corresponds to E_{CORR} in a 3M HCl solution (Figure 21). A further decrease in the applied potential will reduce protons in the crevice to hydrogen thus increasing the pH inside the crevice. The pH will evolve with applied potential following the E_{CORR} curve in Figure 21. When the pH value corresponding to the active to passive transition in deaerated solution (pH = 1.7) is reached, crevice corrosion will stop since active dissolution cannot exist in these conditions. This potential of about -0.270 V_{SCE} can be considered the minimum limit for the repassivation potential in chloride solutions at 90ºC. This repassivation potential is consistent with reported data in literature since the minimum repassivation potential found for a concentrated chloride solution was -0.223 V_{SCE} for 5M $CaCl_2$ at 90ºC[24].

CONCLUSIONS

1. Geometrical conditions in a propagating crevice may be different from those of a developing pit. In the first case the effective diffusion distance (x^2/g) into the pit is increased by corrosion while in the latter x^2/g into the crevice is decreased by corrosion. Decreasing x^2/g accounts for crevice corrosion stifling or repassivation observed[21] on Alloy 22 after long anodic polarization.

2. Differences between breakdown and repassivation potentials of crevice corrosion in CPP[23] can be attributed to the potentiodynamic nature of the scan, taking into account the effect of potential in crevice corrosion incubation time. The breakdown potential is expected to decrease approaching repassivation potential for low scan rates.

3. The crevice corrosion current density was found to be a function of applied potential. i_{CREV} values ranged from 40 μA/cm^2 to 20 mA/cm^2. Such low values explained the absence of pitting corrosion in Alloy 22 at any potential as the critical conditions for localized acidification to occur ($x.i > (x.i)_{CRIT}$) cannot be reached by passive film rupture.

4. A minimum limit value for repassivation potential in crevices with $x^2/g \to \infty$ is proposed to be the minimum corrosion potential of Alloy 22 in hydrochloric acid solutions at which active corrosion exists.

AKNOWLEDGEMENTS

This work was performed under the auspices of the U. S. Department of Energy (DOE) by the University of California Lawrence Livermore National Laboratory under contract N° W-7405-Eng-48, and supported by the Yucca Mountain Project, which is part of the Office of Civilian Radioactive Waste Management (OCRWM).

R. M. Carranza acknowledges financial support from the Agencia Nacional de Promoción Científica y Tecnológica of the Ministerio de Educación, Ciencia y Tecnología from Argentina.

DISCLAIMER

any of their employees, makes any warranty, express or implied, or assumes any legal liability or responsibility for the accuracy, completeness, or usefulness of any information, apparatus, product, or process disclosed, or represents that its use would not infringe privately owned rights. Reference herein to any specific commercial product, process, or service by trade name, trademark, manufacturer, or otherwise, does not necessarily constitute or imply its endorsement, recommendation, or favoring by the United States Government or the University of California. The views and opinions of authors expressed herein do not necessarily state or reflect those of the United States Government or the University of California, and shall not be used for advertising or product endorsement purposes.

REFERENCES

1 ASTM International, Annual Book of ASTM Standards, Volume 03.02 "Corrosion of Metals" (West Conshohocken, PA: ASTM International, 2002).

2 R. B. Rebak in Corrosion and Environmental Degradation, Volume II, (Wiley-VCH, 2000: Weinheim, Germany).

3 A. I. Asphahani, The Arabian Journal of Science and Engineering Vol. 14, Nº2 pp. 317-335 (1989).

4 P. E. Manning, J. D. Smith, and J. L. Nickerson, Materials Performance, pp. 67-73, June 1988.

5 A. Boniface, The Chemical Engineer, No. 477, p. 21 (July 1990).

6 G. M. Gordon, Corrosion, Vol. 58 Nº 10, p. 811 (2002).

7 Proceedings from an Intl. Workshop on Long-Term Passive Behavior, 19 and 20 July, Arlington, Virginia, ed. A. A. Sagüés and C. A. W. Di Bella, USNWTRB, 2001.

8 Waste Package Materials Performance Peer Review, A Compilation of Special Topic Reports, Compiled and Edited by F. M. G. Wong and J. H. Prayer, 2002.

9 R. B. Rebak, Paper 05610 Corrosion/2005, NACE Intl. 2005: Houston, TX.

10 K. A. Gruss, G. A. Cragnolino, D. S. Dunn and N. Sridhar; Paper 149 Corrosion/1998, NACE Intl. 1998: Houston, TX.

11 B. A. Kehler, G. O. Ilevbare and J. C. Scully, Corrosion, Vol. 57 Nº 12 p. 1042 (2001).

12 K. J. Evans, and R. B. Rebak, Corrosion Science a Retrospective and Current Status in Honor of R. P. Frankenthal, The Electrochemical Society 2002, Pennington, New Jersey, 2002-13, pp. 344-354.

13 R. B. Rebak and J. C. Estill in Fall Meeting of the Materials Research Society, Boston, Massachusetts, 2-6 December 2002, Vol. 757, Paper II4.1, pp 713-721.

14 R. B. Rebak, T. S. E. Summers, T. Lian, R. M. Carranza, J. R. Dillman, T. Corbin and P. Crook, Paper 02542, Corrosion/02, NACE Intl. 2002, Houston, TX.

15 K. J. Evans, S. D. Day, G. O. Ilevbare, M. T. Whalen, K. J. King, G. A. Hust, L. L. Wong, J. C. Estill and R. B. Rebak, Transportation, Storage and Disposal of Radioactive Materials, PVP-Vol. 467, p. 55 (ASME, 2003: New York, NY)

16 V. Jain, D. S. Dunn, N. Sridhar and L. Yang, Paper 03690, Corrosion/03, NACE Intl. 2003, Houston, TX.

17 D. S. Dunn, L. Yang, C. Wu and G. A. Cragnolino, Mat. Res. Soc. Symp. Proc. Vol 824 (MRS, 2004: Warrendale, PA)

18 D. S. Dunn, Y.-M. Pan, K. Chiang, L. Yang, G. A. Cragnolino and X. He, JOM, January 2005, pp 49-55.

19 D. S. Dunn, Y.-M. Pan, L. Yang, G. A. Cragnolino, Corrosion, Vol.61 Nº 11 p. 1078 (2005).

20 K. J. Evans, A. Yilmaz, S. D. Day, L. L. Wong, J. C. Estill and R. B. Rebak, JOM, January 2005, pp 56-61.

21 A. Yilmaz, P. Pasupathi and R. B. Rebak, Paper PVP2005-71174, ASME Pressure Vessels and Piping Conference, 17-21 July 2005, Denver, CO (ASME, 2005: New York, NY).

22 M. A. Rodríguez, R. M. Carranza and R. B. Rebak, Met. Trans. A Vol. 36A-No.5, 2005, pp. 1179-1185.

23 R. M. Carranza, M. A. Rodríguez and R. B. Rebak, Paper 06626, Corrosion/06 NACE Intl. 2006, Houston, TX.

24 R. M. Carranza, M. A. Rodríguez and R. B. Rebak, submitted to Corrosion Journal.

25 P. Combrade in Corrosion Mechanisms in Theory and Practice p. 349, Second Edition, edited by P. Marcus (Marcel Dekker 2002, New York, NY).

26 H. W. Pickering, Journal of The Electrochemical Society, 150 (5) pp. K1-K13, 2003.

27 J. S. Lee, M. L. Reed and R. G. Kelly, Journal of The Electrochemical Society, 151 (7) pp. B423-B433, 2004.

28 M. Vankeerberghen, Corrosion Vol. 60 Nº 8, p. 707 (2004).

29 Z. Szklarska-Smialowska, Pitting and Crevice Corrosion of Metals, NACE Intl. Houston TX, 2005. (Chapter 19, pp. 459-497).

30 M. A. Rodríguez, Ms. Sc. Thesis, University of General San Martín, Argentina (2003).

31 N. Sridhar and G. A. Cragnolino, Corrosion Vol. 49 Nº 11, p. 885 (1993).

32 B. E. Wilde and E. Williams, Electrochimica Acta, 16 pp.1071-1085,1971.

33 J. R. Galvele, Journal of The Electrochemical Society, 123 (4) pp. 464-474, 1976.

34 J. R. Galvele, Corrosion Science 21 (8) pp. 551-579, 1981.

35 S. M. Gravano and J. R. Galvele, Corrosion Science 24 (6) pp. 517-534, 1984.

36 J. R. Galvele, J. B. Lumsden and R. W. Staehle, Journal of The Electrochemical Society, 125 (8) pp. 1204-1208, 1978.

37 R. C. Newman, M. A. A. Ajawi, H. Ezuber, S. Turgoose, Corrosion Science 28 (5) pp. 471–477, 1988.

38 R. C. Newman, Corrosion Science 25 (5) pp. 331–339, 1985.

39 R. C. Newman, Corrosion Science 25 (5) pp. 341–350, 1985.

40 R. S. Lillard, M. P. Jurinski and J. R. Scully, Corrosion Vol. 50 Nº 4, p. 251 (1994).

41 M. Pourbaix, Atlas of Electrochemical Equilibria in Aqueous Solutions, NACE Intl. Houston, TX, 2nd ed.1974.

42 R. B. Rebak and P. Crook, PVP-Vol. 483 Transportation, Storage and Disposal of Radioactive Materials, pp. 131-136 (ASME, 2004: New York, NY)

43 R. M. Carranza, M. A. Rodríguez and R. B. Rebak, Unpublished results.

TABLE 1

RELEVANT DATA FROM ELECTROCHEMICAL TESTS FOR ALLOY 22 PCA SPECIMENS IN DEAERATED pH 2, 1M NaCl AT 90ºC.

Applied Potential, V_{SCE}	**Corroded Area[(1)], cm^2**	**Polarization hold time, s**	**EIS starting time, s**	**Circulated Charge[(2)], C/cm^2**	**Maximum depth[(3)], µm**	**Calculated depth[(4)], µm**
-0.200	No CC	36000	-	-	-	-
-0.180	No CC	94000	-	-	-	-
-0.170	0.30	82700	77400	0.032	< 5	0.4
-0.140	0.30	87100	88900	0.108	< 5	1.4
-0.100	0.43	17500	15500	0.029	< 5	0.3
0.000	0.53	18700	16100	0.23	< 5	1.7
0.100	0.45	17800	15700	0.56	20	4.8
0.200	0.60	15900	14700	0.89	70	5.8
0.300	0.67	12400	8900	5.0	200	29.3
0.400	0.53	12400	8900	3.8	260	28.1
0.500	0.64	12400	8900	6.6	250	38.5
0.600	0.75	12400	8900	7.2	180	37.1
0.700	0.69	12600	9000	3.1	170	17.5

(1) Corroded area in the crevice calculated by using an image processing software.
(2) Circulated anodic charge during potentiostatic hold plus potentiodynamic polarization normalized by the total area of the specimen.
(3) Maximum depth found in the crevice corroded area by optical microscopic observations.
(4) Depth of attack in the crevice corroded area (average value) assuming that the crevice corrosion penetration was even. Assumptions: congruent dissolution of the major alloying elements; all the circulated anodic charge was due to corrosion attack in the calculated corroded area.
CC: crevice corrosion

TABLE 2

ATOMIC PERCENT OF ELEMENTS DETECTED BY EDX ANALYSIS IN PRECIPITATES FOUND ON LOCALIZED ATTACKED AREAS IN PCA SPECIMENS IN DEAERATED pH 2, 1M NaCl AT 90ºC.

E, V_{SCE}	Mo	Si	Cl	Cr	Mn	Fe	Ni	W
-0.170	33.56	ND	5.61	25.75	1.50	3.06	23.28	7.25
-0.140	38.67	ND	8.96	22.47	1.49	ND	17.07	11.34
-0.100	38.60	ND	6.10	20.95	1.58	2.71	20.75	9.31
0.000	43.06	ND	6.56	15.60	1.93	2.69	17.00	13.17
0.100	29.54	11.23	6.62	19.57	1.42	2.65	20.64	8.33
0.200	44.97	ND	7.66	14.74	2.19	3.05	15.27	12.12
0.300	24.80	7.00	3.99	19.28	1.36	3.15	35.84	4.59
0.400	19.80	7.50	5.00	23.82	1.24	3.12	34.92	4.62
0.500	25.72	9.84	5.21	20.33	1.30	2.89	28.57	6.16
0.600	32.34	ND	4.96	24.68	1.11	2.72	29.19	5.01
0.700	22.40	7.41	3.11	20.28	1.21	3.01	37.86	4.71
0.700	35.40	16.47	9.11	12.52	1.79	2.52	10.01	12.19

TABLE 3

RATIO OF ATOMIC PERCENT OF THE ELEMENT DETECTED IN PRECIPITATES AND ATOMIC PERCENT OF THE ELEMENT NOMINALLY PRESENT IN ALLOY 22.

Atomic % Me in Precipitate / Atomic % Me in Alloy 22					
E, V_{SCE}	Ni	Cr	Mo	W	Fe
-0.170	0.41	1.07	4.36	7.82	1.00
-0.140	0.30	0.94	5.03	12.27	ND
-0.100	0.36	0.87	5.02	10.05	0.89
0.000	0.30	0.66	5.65	14.35	0.90
0.100	0.42	0.94	4.41	10.32	1.00
0.200	0.28	0.63	6.02	13.48	1.03
0.300	0.67	0.85	3.42	5.25	1.09
0.400	0.66	1.07	2.78	5.38	1.10
0.500	0.56	0.94	3.71	7.38	1.05
0.600	0.50	1.01	4.13	5.32	0.88
0.700	0.70	0.89	3.06	5.35	1.04
0.700	0.22	0.67	5.89	16.83	1.05
Average	0.45	0.88	4.46	9.48	1.00

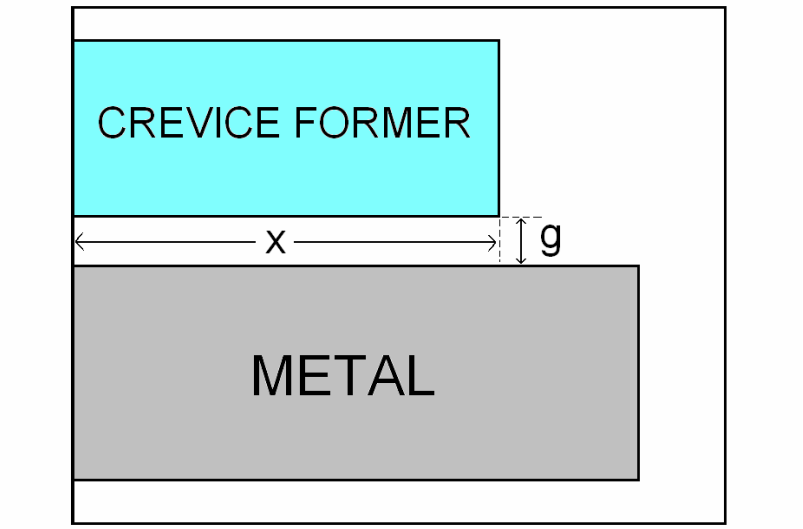

FIGURE 1: Schematic representation showing the two characteristic dimensions of a crevice: crevice depth (x) and crevice gap (g).

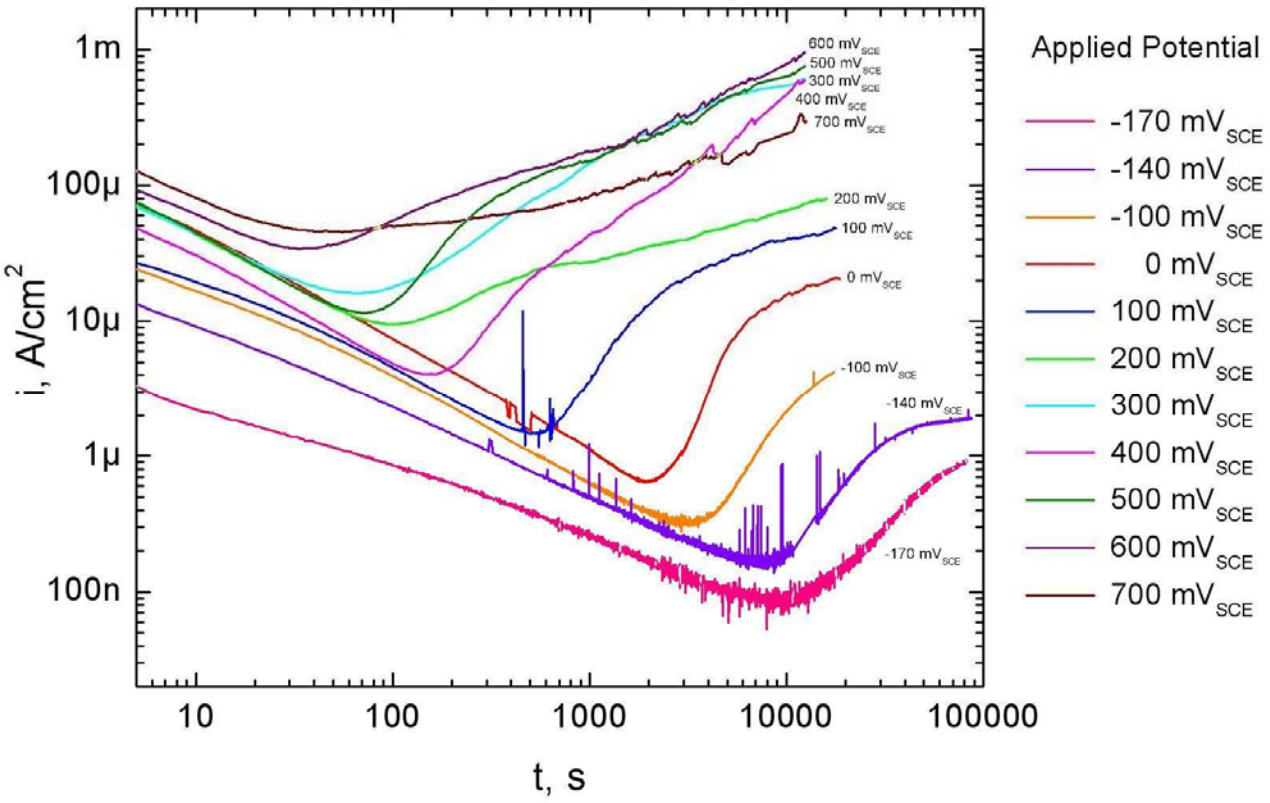

FIGURE 2: Potentiostatic curves obtained for Alloy 22 PCA specimens in deaerated pH 2, 1M NaCl solutions at different applied potentials and 90ºC.

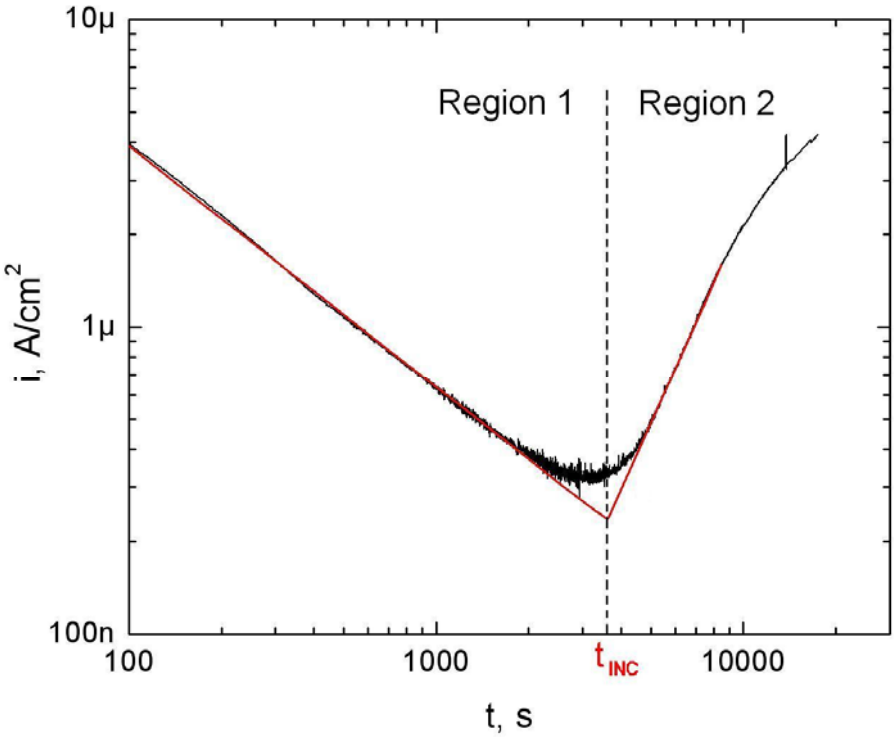

FIGURE 3: Potentiostatic curve obtained for a Alloy 22 PCA specimen in deaerated pH 2, 1M NaCl solutions at -100 mV_{SCE} and 90ºC. Linear fittings for regions 1 and 2 are also shown. Incubation time (t_{INC}) for crevice corrosion is defined at the intersection of these linear fittings.

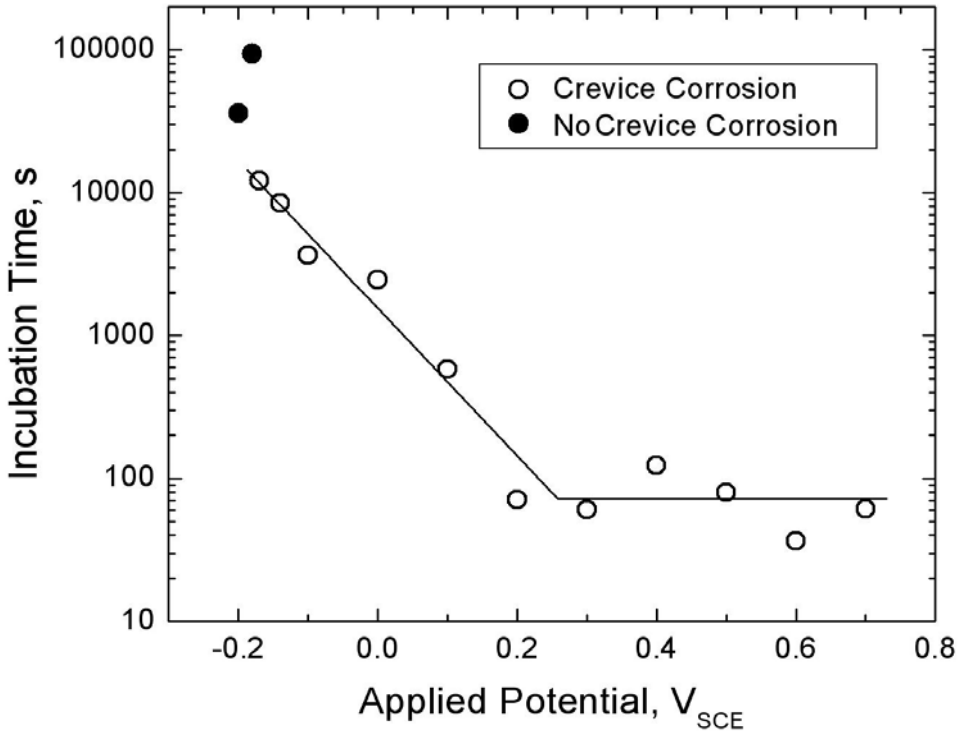

FIGURE 4: Incubation time for crevice corrosion as a function of applied anodic potential for Alloy 22 PCA specimens in deaerated pH 2, 1M NaCl solutions and 90ºC.

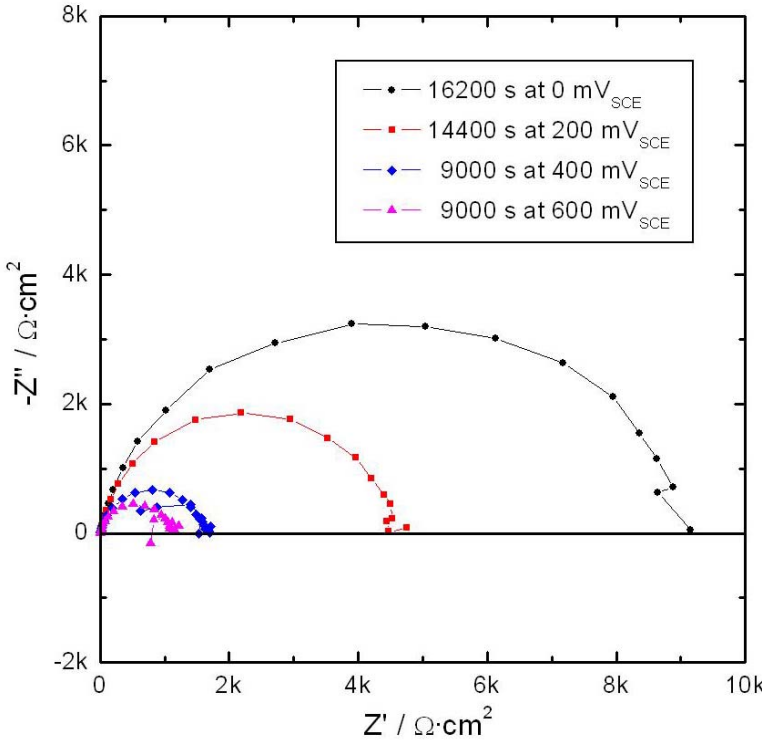

FIGURE 5: Complex plane impedance plots for EIS measurements at different applied potentials and polarization times for Alloy 22 PCA specimens in deaerated pH 2, 1M NaCl solutions and 90ºC.

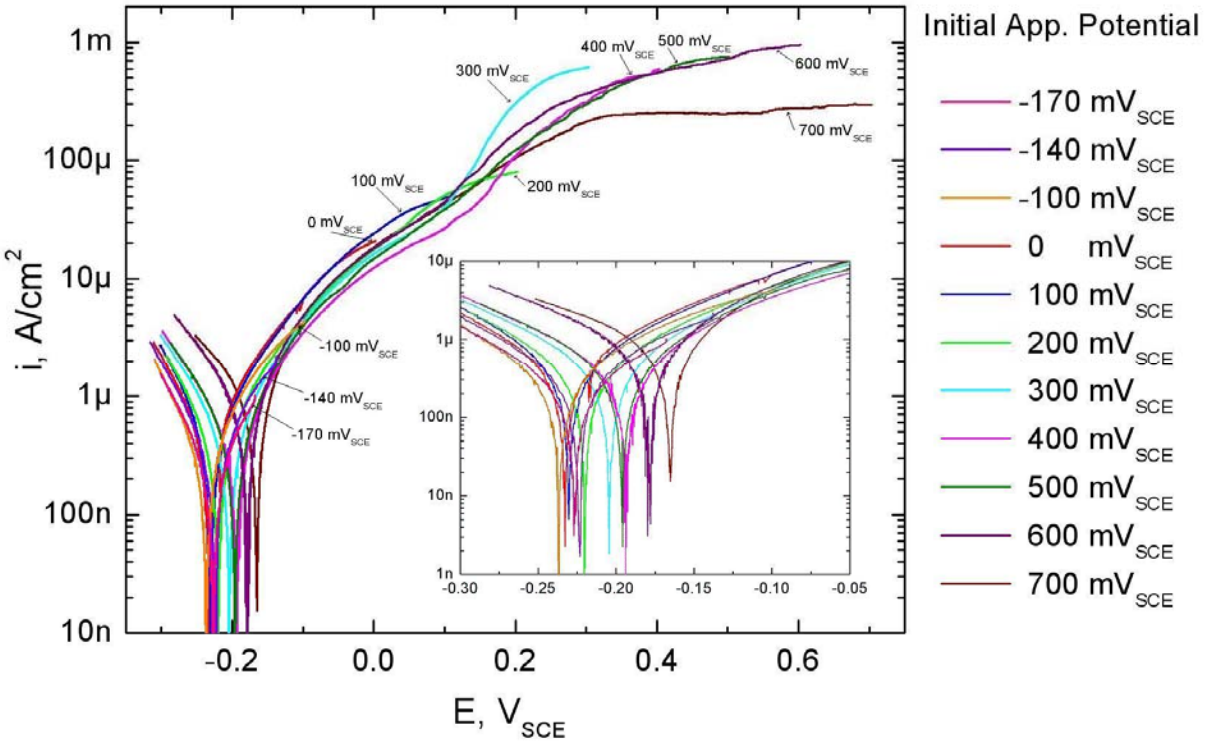

FIGURE 6: Repassivation curves: Potentiodynamic polarization curves in the cathodic direction after different initial applied potentials (Fig. 2) for Alloy 22 PCA specimens in deaerated pH 2, 1M NaCl solutions at 90ºC.

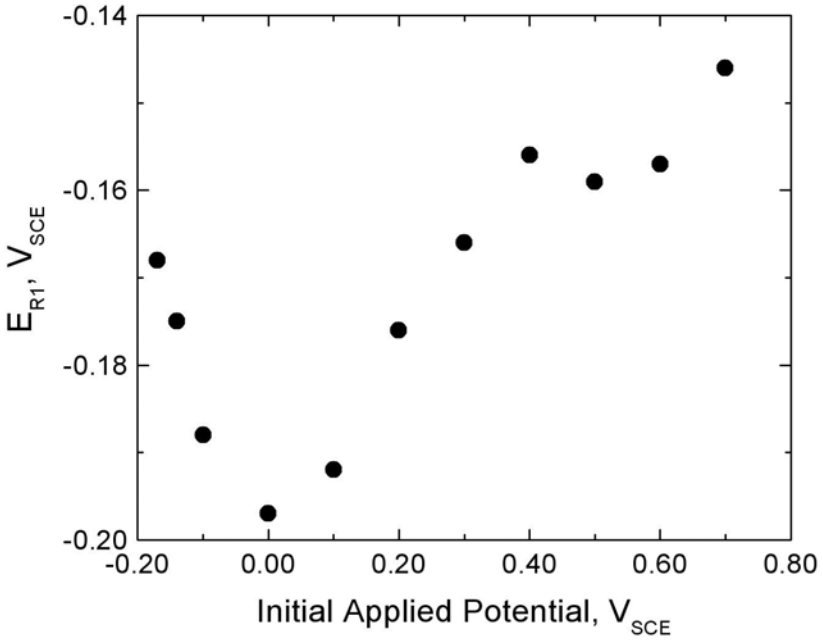

FIGURE 7: Repassivation potential (E_{R1}) obtained from repassivation curves (Fig. 6) as a function of initial applied potential for Alloy 22 PCA specimens in deaerated pH 2, 1M NaCl solutions at 90ºC.

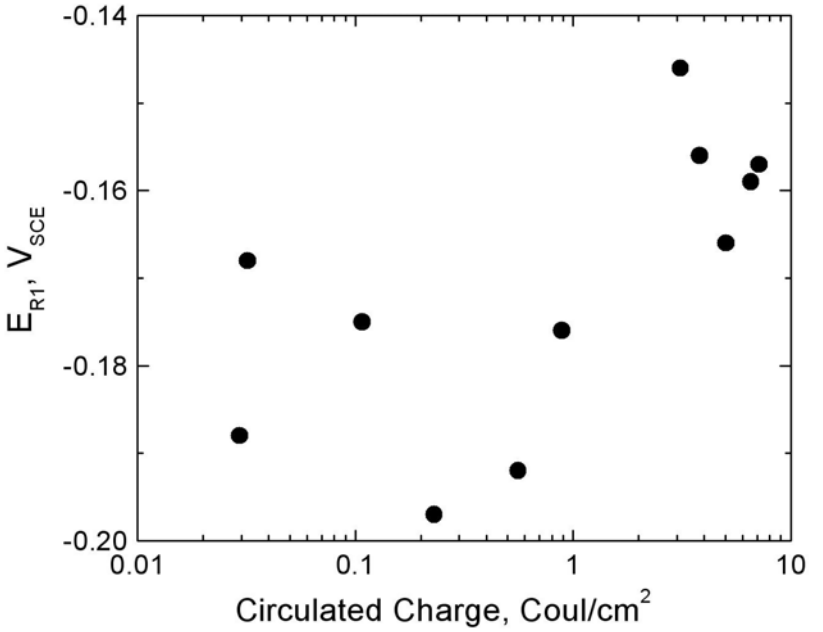

FIGURE 8: Repassivation potential (E_{R1}) from repassivation curves (Fig. 6) as a function of total circulated charge for Alloy 22 PCA specimens in deaerated pH 2, 1M NaCl solutions at 90ºC.

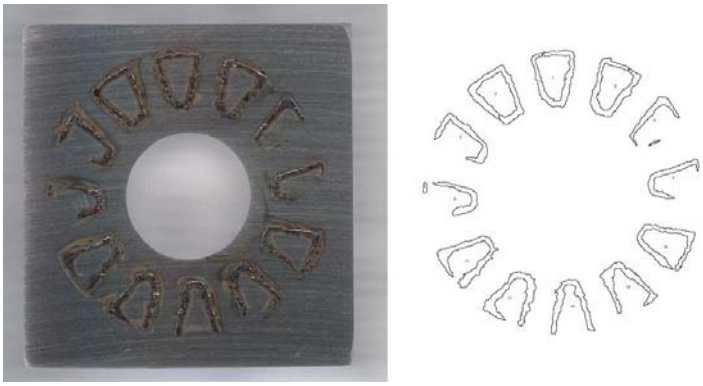

a) Side 1: Corroded surface under the PTFE-wrapped ceramic washer

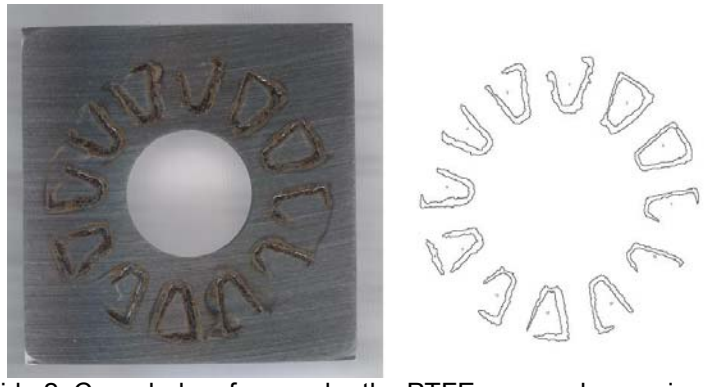

b) Side 2: Corroded surface under the PTFE-wrapped ceramic washer

FIGURE 9: Photographs of an Alloy 22 PCA specimen tested at 100 mV_{SCE} along with its corresponding contours of the creviced corroded areas obtained by using an image processing software.

a)Side 1: Corroded surface under the PTFE-wrapped ceramic washer

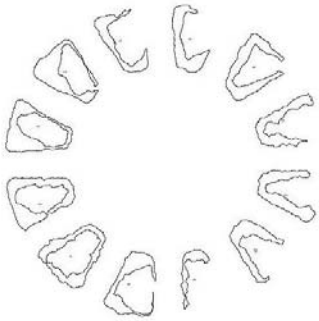

b)Side 2: Corroded surface under the PTFE-wrapped ceramic washer

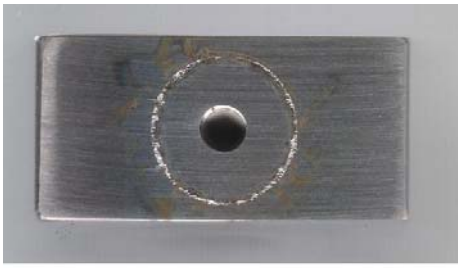

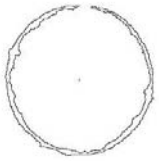

c) Upper Side: Corroded surface under a PTFE compression gasket

FIGURE 10: Photographs of Alloy 22 PCA specimen tested at 500 mV_{SCE} along with corresponding contours of the creviced corroded areas obtained by using an image processing software.

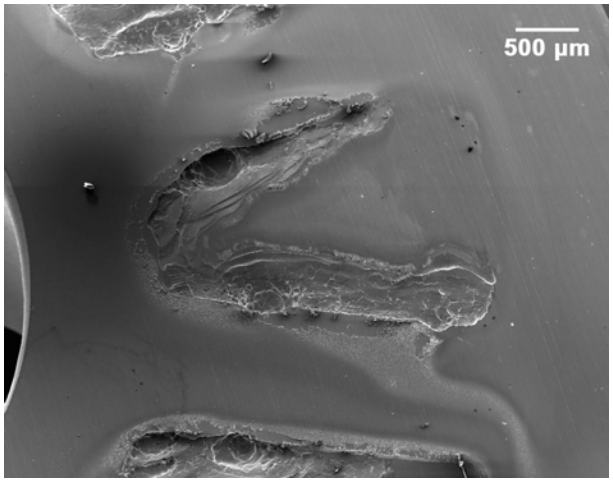

FIGURE 11: SEM image of an Alloy 22 PCA specimen tested at 500 mV_{SCE}.
Original magnification 25X

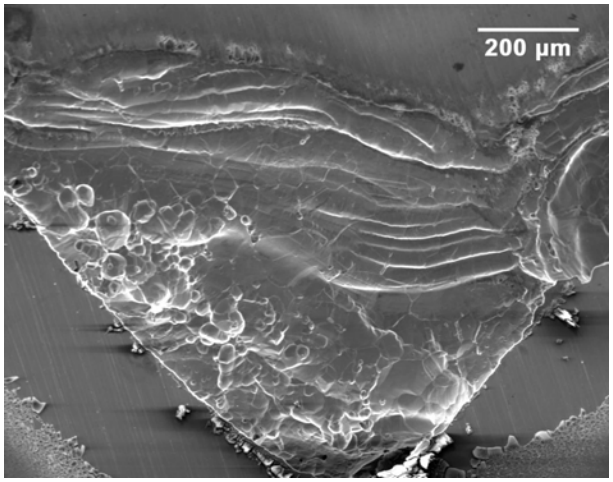

FIGURE 12: SEM image of an Alloy 22 PCA specimen tested at 500 mVSCE.
Original magnification 100X

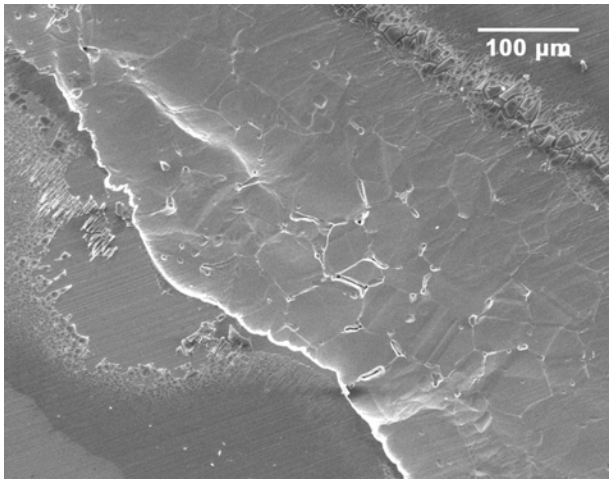

FIGURE 13: SEM image of an Alloy 22 PCA specimen tested at 200 mV_{SCE}.
Original magnification 200X

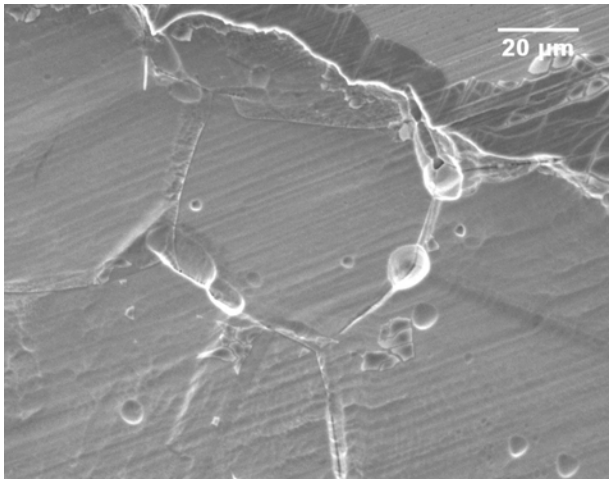

FIGURE 14: SEM image of an Alloy 22 PCA specimen tested at 200 mV_{SCE}.
Original magnification 800X

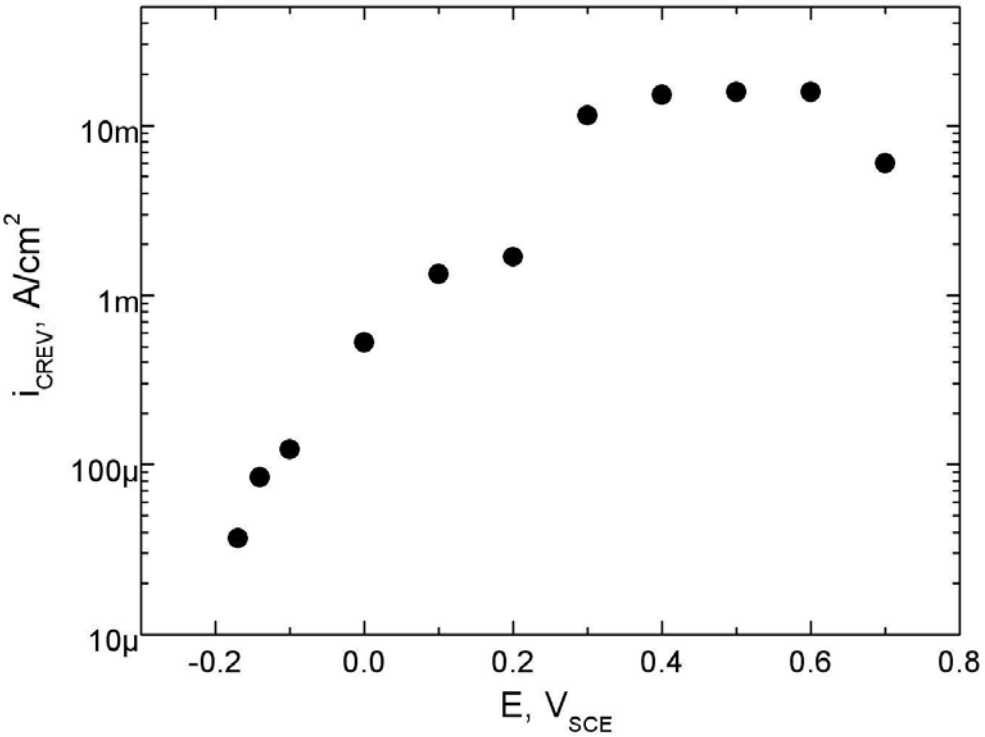

FIGURE 15: Current density in the crevice (i_{CREV}) as a function of applied potential for or Alloy 22 PCA specimens in deaerated pH 2, 1M NaCl solutions at 90ºC.

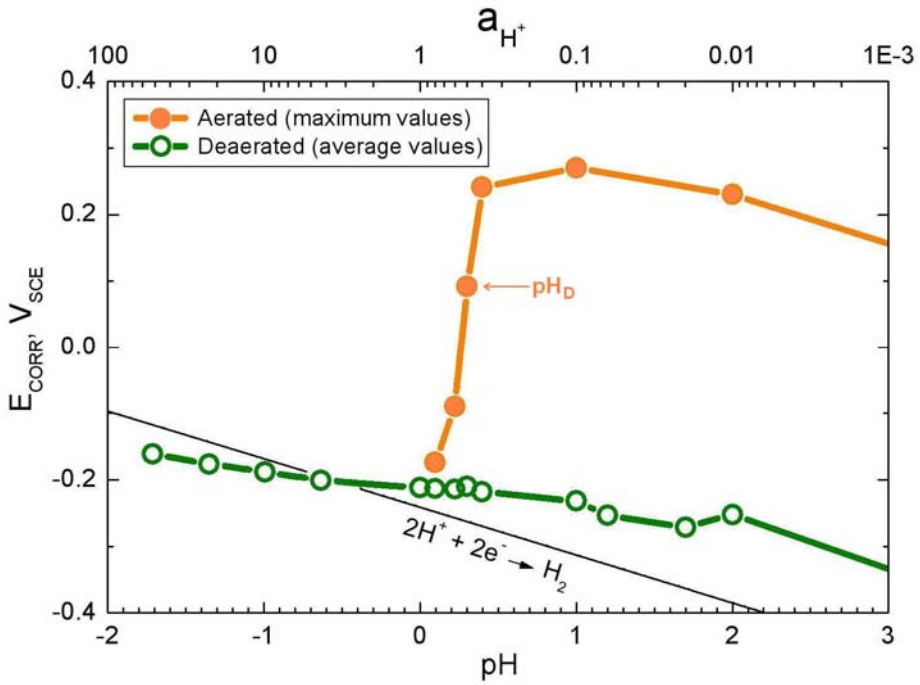

FIGURE 16: Corrosion potential (E_{CORR}) for Alloy 22 prismatic specimens tested in aerated and deaerated chloride solutions as a function of pH or proton activity (a_{H^+}) at 90ºC. Maximum reached values are shown for aerated solutions and average values are shown for deaerated solutions. pH values for 1M to 5M HCl solutions were corrected on account of chloride effect on proton activity.[40]

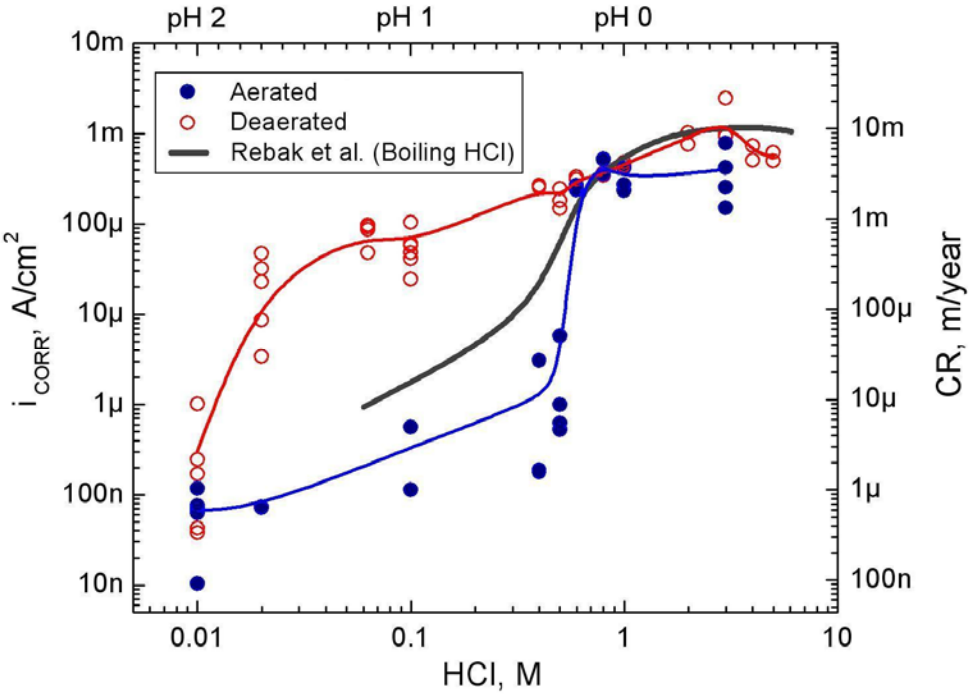

FIGURE 17: Corrosion current density (i_{CORR}) and corrosion rate (CR) for Alloy 22 prismatic specimens determined from EIS measurements at different immersion times in low pH chloride solutions at 90ºC as a function of hydrochloric acid concentration or pH. Results of Rebak *et al.* [42] in boiling hydrochloric acid are also shown.

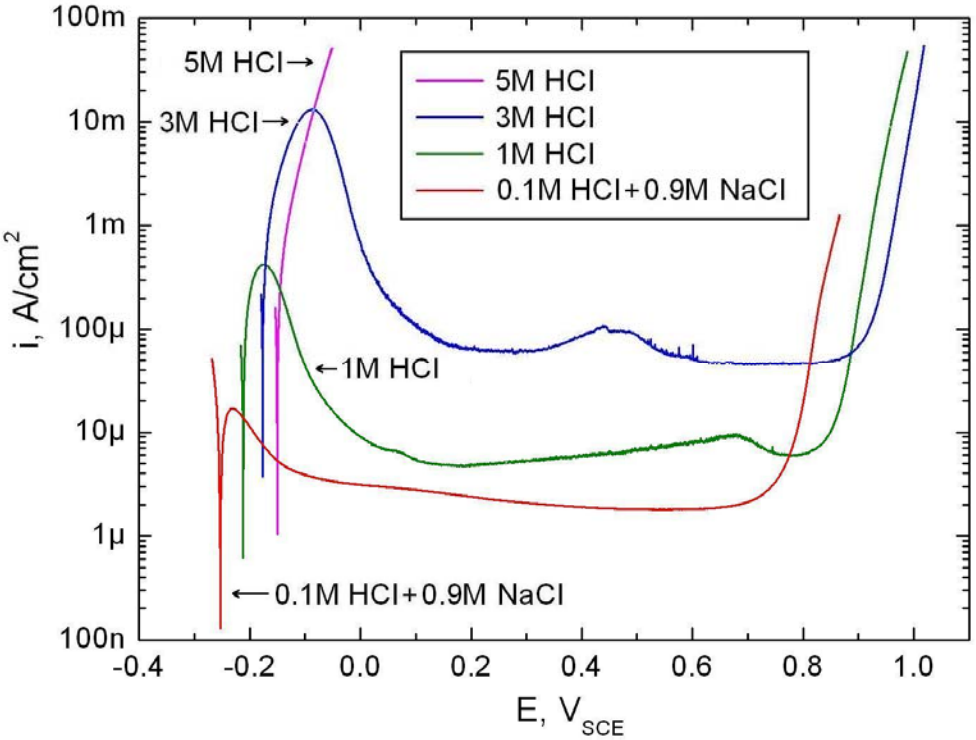

FIGURE 18: Potentiodynamic polarization curves for Alloy 22 prismatic specimens in deaerated hydrochloric acid solutions of different concentrations at 90ºC. Scan rate 0.167 mV/s.

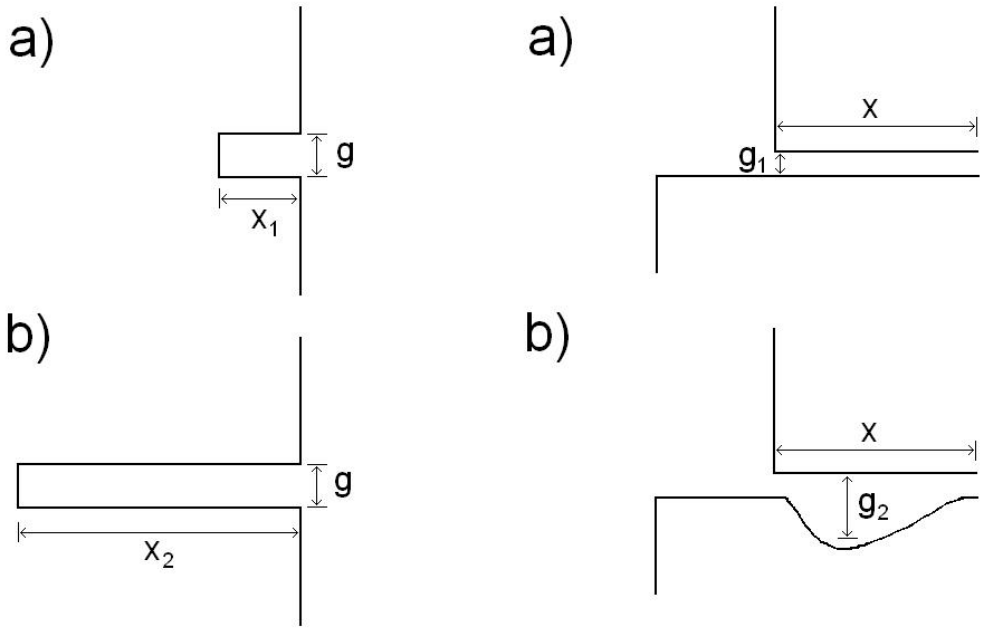

FIGURE 19: Schematic representation of a two-stage localized corrosion process in a deep pit (left) and in a crevice (right).

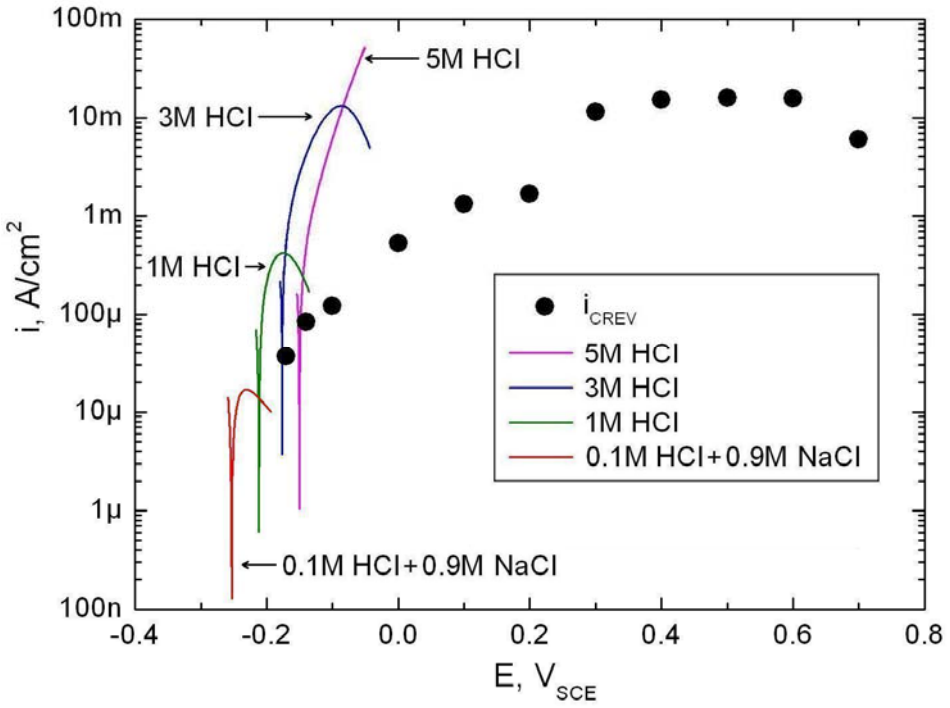

FIGURE 20: Current density in the crevice (i_{CREV}) as a function of applied potential for or Alloy 22 PCA specimens in deaerated pH 2, 1M NaCl solutions at 90ºC and active range of potentiodynamic polarization curves for Alloy 22 prismatic specimens in deaerated hydrochloric acid solutions of different concentrations.

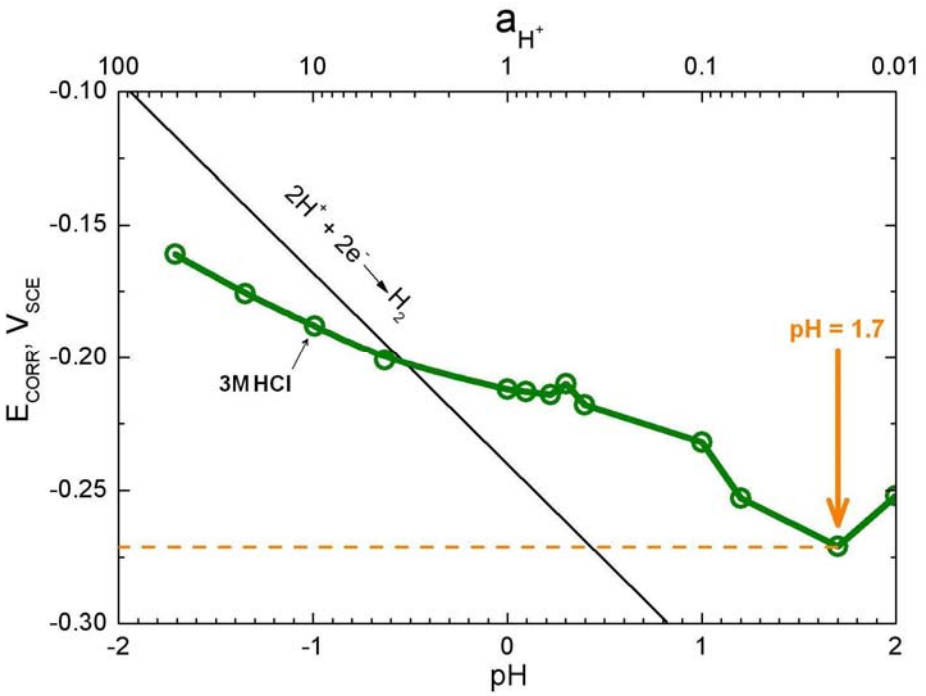

FIGURE 21: Corrosion potential (E_{CORR}) for Alloy 22 prismatic specimens tested in deaerated chloride solutions as a function of pH or proton activity (a_{H^+}) at 90ºC. Average values are shown (Fig. 16). pH values for 1M to 5M HCl solutions were corrected on account of chloride effect on proton activity.[40]